Shahid Bahonar University of Kerman

Biomechanism and Bioenergy Research

Online ISSN: 2821-1855
Homepage: https://bbr.uk.ac.ir

Iranian Society of Agricultural Machinery Engineering and Mechanization

Differentiating Alternaria Species Using Hyperspectral Imaging

Mohammad Hossein Nargesi[1], Khadijeh Abbasi[2]✉, Parisa Karami[2], Kamran Kheiralipour[1]

[1] Mechanical Engineering of Biosystems, Department, Ilam University, Ilam, Iran.
[2] Plant Protection Department, Ilam University, Ilam, Iran.

✉ Corresponding author: kh.abasi@ilam.ac.ir

ARTICLE INFO

Article type:

Research Article

Article history:

Received 28 April 2025

Received in revised form 04 June 2025

Accepted 01 September 2025

Available Online 30 September 2025

Keywords:

Enzyme activity, Fungi, Principal component analysis, Spectral reflectance processing.

ABSTRACT

Rice is one of the most important cereal crops. This plant is native to tropical and subtropical regions and has the largest cultivated area in the world after wheat. Rice is exposed to various types of biotic and abiotic stresses at different stages of cultivation. Among the different pathogens, fungi have the largest pathogenicity spectrum. Hyperspectral imaging is used specifically in assessing the safety and quality of food. The present study demonstrates the possibility of using hyperspectral imaging to differentiate *Alternaria* species. The samples used in the study included *A. solani*, *A. dumosa*, and *A. atra*. Hyperspectral images of the samples were obtained using a scanning imaging system. The effective wavelengths were selected using principal component analysis (PCA). According to the principal component analysis, the increase in time was associated with enhanced enzymatic activity, which led to a lighter color of the solution. Moreover, a significant difference in enzyme activity levels was observed across the different days. Also, fungal growth increased with increasing enzyme activity duration. Also, in the comparison between different fungal isolates, significant differences were observed between different isolates.

Cite this article: Nargesi, M. H., Abbasi, Kh., Karami, P., & Kheiralipour, K (2025). Differentiating Alternaria Species Using Hyperspectral Imaging. *Biomechanism and Bioenergy Research*, *4*(3), 1-10. https://doi.org/10.22103/bbr.2025.25176.1121

Publisher: Shahid Bahonar University of Kerman
DOI: https://doi.org/10.22103/bbr.2025.25176.1121

INTRODUCTION

Rice (*Oryza sativa* L.) is one of the most strategically important agricultural crops worldwide. It is ranked as the second most consumed staple food after wheat. Despite its widespread cultivation, rice production in rainfed areas faces significant constraints due to drought stress, leading to yield instability (Gallé & Katzenberger, 2025) and fluctuations in market supply and demand (Nahar et al., 2018). After wheat, it has the highest cultivation area in the world. It constitutes the food of more than half of the world's population, especially developing countries (Bandumula, 2018; Kunjaroenruk et al., 2025).

Rice is exposed to various types of biotic and abiotic stresses at different stages of cultivation; among the various pathogens, fungi have the largest spectrum of pathogenicity, with rice being attacked by 56 fungal pathogens (Butt et al., 2011). The most important fungal pathogens of rice include *Pyricularia oryzae, Bipolaris orzyae, Gibberella moniliformis, Rhizoctonia solani, Alternaria alternata, Curvularia lunata, and Sarocladium oryzae*. *Curvularia* species are destructive pathogens of grasses and rice. Leaf spot symptoms, characterized by annular necrosis on rice leaves, are of the most common symptoms caused by these fungi in rice fields, which significantly reduce rice yield and productivity (Kusai et al., 2016). Early detection of diseases and differentiation of spots and lesions can lead to the adoption of specific strategies to manage these pathogens, which can prevent a decrease in the quality and quantity of rice yield (Terensan et al., 2021).

Imaging is a non-destructive and a fast, cheap, accurate, and simple (no need to skilled persons) technique that is widely used in various fields (Farokhzad et al., 2024; Hosainpour et al., 2022; Khazaee et al., 2022; Kheiralipour et al., 2013; Kheiralipour & Nargesi, 2024; Nargesi et al., 2024; Nargesi et al., 2025; Nargesi & Kheiralipour, 2024a, 2024b). Hyperspectral imaging (HSI) or chemical imaging is one of the new techniques in this field that combines the advantages of spectroscopy as an analytical tool with the two-dimensional object visualization provided by optical imaging (Kheiralipour & Jayas, 2023). In this technique, spectral information of each pixel is recorded. This information is added as a third dimension containing reflectance values to the two-dimensional spatial image to create a three-dimensional data cube, which is referred to as the image cube or hypercube. Hyperspectral imaging, which captures electromagnetic waves in the visible (Vis) and near-infrared (NIR) wavelength ranges, is a new imaging technique. It has been used to evaluate various materials (Kheiralipour & Jayas, 2023; Kumar et al., 2016; Liu et al., 2020; Vejarano et al., 2017). The ability to detect targets in the invisible spectrum, which cannot be observed using visible imaging, is a key factor that distinguishes hyperspectral imaging from visible imaging (Kheiralipour & Jayas, 2023; Kheiralipour & Nargesi, 2024).

HSI technique has a wide range of applications in agriculture and the food industry (Kheiralipour & Jayas, 2023). Fungal contamination in various agricultural products has been detected using hyperspectral imaging technology (Kheiralipour et al., 2015; Kheiralipour et al., 2021). The objective of this study is to differentiate fungal species associated with rice contamination using hyperspectral imaging technique as an innovative approach that has not yet been applied in this field. Also, fungus growing days has been differentiated using HSI in the present research.

MATERIALS AND METHODS

Sample Preparation

The first step in the present study was to prepare experimental samples. The samples were collected from different fields in Ilam province, Iran. The fungal species utilized in this study included *A. solani, A. dumosa, and A. atra* (Figure. 1a).

Production and Induction of Chitinase Enzyme

Substrate preparation

Colloidal chitin as a substrate to prepare a culture medium for inducing the chitinase enzyme was prepared following the procedure of Tikhonov et al. (Tikhonov et al., 2002). To prepare colloidal chitin, 100 ml of 85% phosphoric acid was added to ten grams of chitin powder and the resulting mixture was kept at 4°C for 24 hours. Water was added to the mixture and filtered with filter paper. To completely remove the acid, the steps of adding water and filtering were repeated several times. The resulting paste was dried and powdered and used as a carbon source in the water agar medium.

Preparation of induction culture medium

To prepare the basic culture medium for the production of chitinase enzyme, five-mm-diameter discs were cultured from five-day-old isolates in MSM liquid culture medium containing (NH4)2SO4: 2.8 g, Urea: 0.6 g, KH2PO4: 4 g, Cacl2.2H2O: 0.6 g, MgSO4: 0.2 g, FeSO4.7H2O: 0.01 g, ZnSO4.H2O: 0.0028 g, Cocl2.6H2O: 0.0032 g, and one gram per liter of colloidal chitin. In this way, 100 ml of the culture medium was poured into 250 ml Erlenmeyer flasks and placed on a shaker for five days at a speed of 120 rpm and a temperature of 25 °C (Abbasi et al., 2017).

Investigation of chitinase enzyme activity

To prepare the chitin base solution, 0.5% colloidal chitin was dissolved in 100 ml of distilled water. Chitinase activity was determined by measuring the release of reducing saccharides from colloidal chitin by the N-acetyl-glucosamine-dinitrosalicylate method according to the method described by Monreal and Reese (Monreal & Reese, 1969). A reaction mixture containing 200 µl 0.5% chitin provided in citrate phosphate buffer (0.05 M, pH = 6.6) and 200 µl enzyme solution was incubated at 37°C for 1 h. Then 1 ml of dinitrosalicylic acid reagent (DNS) was added to reaction. The reaction was heated in boiling water for 5 min and was centrifuged at 6,000 rpm for 5 min and absorbance at 540 nm for four times; 24 h, 48 h, 72 h and 96 h were measured. The spectrophotometer was zeroed for the samples by the reaction mixture whose extract activity had been stopped in a 100°C water bath.

Evaluation of the ability to produce chitinase enzyme in chitin-agar culture medium

The ability of the fungal isolates to produce chitinase enzyme was investigated in WA medium containing 0.5% colloidal chitin, where chitin is used as the sole carbon source by the fungus. A 5 mm disc from the edge of a 4-day-old fungal culture was placed in the center of the dish and the dishes were kept at 25°C for 5 days. After 5 days, the ability of the isolates to produce chitinase enzyme was evaluated by measuring the diameter of the fungal mycelium.

Hyperspectral Imaging

The imaging step was conducted in Image Processing Laboratory, Ilam University, Ilam, Iran. In the present research, a line scan visible near-infrared (vis-NIR) hyperspectral imaging system (Model Specam, Parto Sanat Co., Zanjan, Iran) with a wavelength range of 400 to 950 nm was used (Fig. 1). The hyperspectral images (hypercubes) of the samples were saved in a personal computer to be processed in the next step.

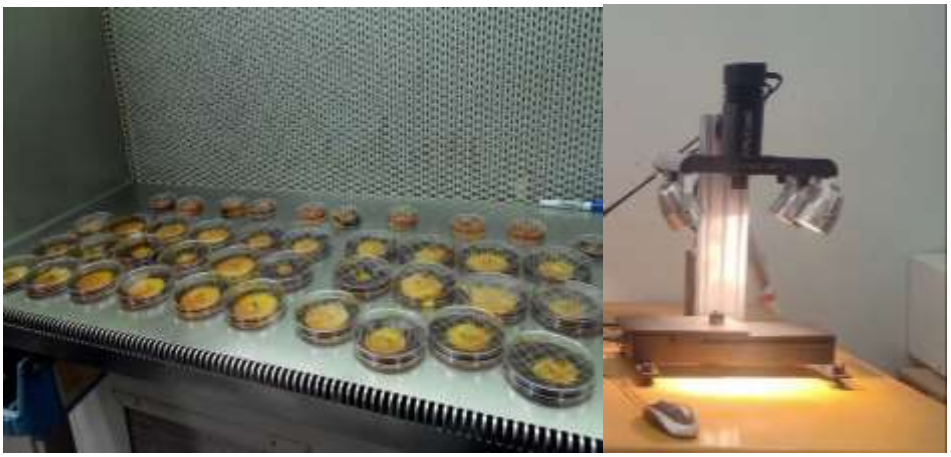

Figure 1. The studied fungal isolates (left) and the used hyperspectral imaging system (right).

Image Processing

MATLAB software was used for processing the acquired images (hypercubes). In preprocessing, the center of the hypercubes was cropped to be used in the next step. Then the effective wavelengths were selected using the principal component analysis (PCA) method. To this end, the average principal component (PC) of all wavelengths were calculated and were plotted. The effective wavelengths were fund as the peak of the diagrams (Nargesi et al., 2025). In the final step, the mean (as an image feature) value of the hypercubes corresponding to the effective wavelengths were extracted to show the differences between fungi spices and growing stage.

RESULTS AND DISCUSSION

The Ability of Producing Chitinase Enzyme in Chitin Agar Medium

Three selected fungal isolates were cultured in chitin agar medium to investigate the production of chitinase enzyme. The chitinase enzyme activity was measured as the diameter of the fungal mycelium in petri dish (Fig. 2). All the isolates studied were able to produce chitinase enzyme and break down and utilize chitin. The results of chitinase enzyme production for three different species of *Alternaria* were that the diameter of the fungal mycelium in the *A. solani* was greater than that of the *A. dumosa* isolate and also greater than that of the *A. atra* isolate. The highest and lowest diameters of the fungal mycelium were related to the *A. solani* and the *A. atra* isolate, respectively. The results showed that the larger diameter of the fungal isolates indicates high chitinase activity.

Imaging Results

Fungal spices

The mean values of the principal components PCA of the hyperspectral images of the samples were plotted for all wavelengths. The PCA data of all samples were presented in diagrams and according to the peaks of the curves, the effective wavelengths were selected. The peaks in the graphs were selected as effective channels and the wavelengths corresponding to these effective channels were found based on the output of the imaging system. In the next subsections the results corresponding to differentiating different fungi and also different days were presented.

The average of PCA data of *A. solani, A. dumosa* and *A. atra* spices were plotted (Fig. 2). Based on the peaks in the diagrams, the effective image channels were selected as 40, 99, 177, 275, 351, 430, 550, and 660. Also, the effective wavelengths corresponding to the selected image channels were 432.65, 481.43, 545.93, 626.96, 689.80, 755.12, 854.34, and 945.29 nm.

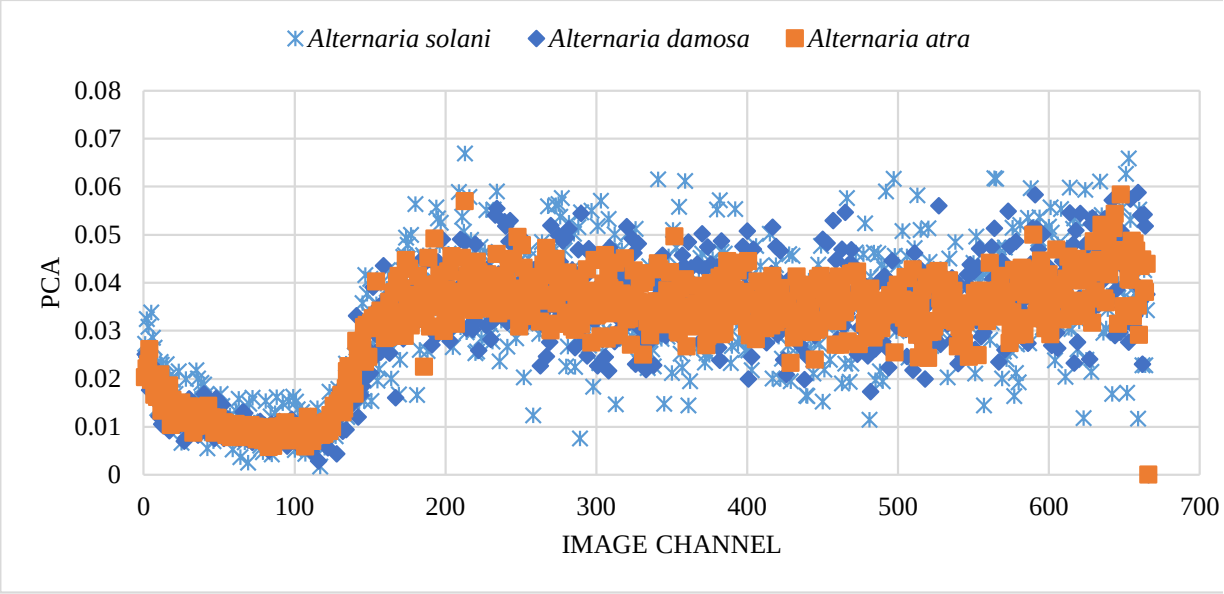

Figure 2. The average PCA diagrams of the studied *Alternaria* species.

The mean of the feature extracted from the hypercubes corresponding to the effective wavelengths for different fungi spices were presented in Table 1. As seen in this table, the mean values of the spices were different from each other. The highest values were obtained for *A. solani* and the lowest values were observed for *A. atra*.

As can be seen in Table 1, the values of the effective wavelength for different species of *A. solani*, *A. dumosa*, and *A. atra* were different. The values for these three species of *A. solani*, *A. dumosa*, *and A. atra*, respectively, had a decreasing trend for all effective wavelengths.

Table 1. Average characteristic value related to effective wavelength for different species, *A. solani, A. dumosa and A. atra*

Wavelength (nm)	*A. solani*	*A. dumosa*	*A. atra*
432.65	0.019	0.017	0.014
481.43	0.016	0.009	0.007
545.93	0.050	0.033	0.031
626.96	0.056	0.050	0.039
689.80	0.051	0.034	0.031
755.12	0.046	0.040	0.032
854.34	0.044	0.042	0.036
945.29	0.055	0.039	0.029

Fungus growing stage

The PCA diagram of related to different growing days of *A. solani*, *A. dumosa*, *A. atra* specieshave been presented in Fig. 3a-c. The effective image channels corresponding to different days for all studied fungi species were selected based on the peaks in the diagrams. Also, the effective wavelengths corresponding to the selected image channels were presented in Table 2.

Figure 3. *Alternaria* fungus with *A. solani* (top), *A. dumosa* (middle), and *A. atra* (bottom) species. D-1 to 4 represent the first to fourth day of fungal growth, respectively.

Table 2. The effective image channels and wavelengths to differentiate different growing days of the studied fungi.

Fungal species	Image channels	Wavelengths
A. solani	186, 198, 285, 368, 392, 510, 518, 560, 596, 598, 633, 649	533.37, 563.29, 581.48, 638.53, 703.85, 779.92, 821.26, 827.88, 862.61, 892.37, 922.97, 936.20.
A. dumosa	383, 549, 552, 584, 591, 614, 626, 630, 631, 632, 638, 648, 659, 663	716.21, 853.51, 855.99, 882.45, 888.24, 907.26, 917.18, 920.49, 921.31, 922.14, 927.10, 935.37, 944.46, and 947.77.
A. atra	461, 555, 617, 621, 631, 641, 644, 655, 656, 658, 660,	780.75, 858.47, 909.74, 913.09, 921.31, 929.58, 932.06, 941.16, 941.98, 943.64, and 945.29.

The values of the mean feature extracted from the hypercubes related to the effective wavelengths for three different species of *A. solani, A. dumosa, and A. atra* at different growing stages were presented in Table 3-5. The highest and lowest values were observed for the first day and fourth day, respectively.

Table 3. The mean feature value corresponding the effective wavelengths for *A. solani* in four days.

W* (nm)	d1	d2	d3	d4
533.37	0.076	0.044	0.036	0.025
563.29	0.062	0.046	0.030	0.001
581.48	0.071	0.068	0.031	0.030
638.53	0.071	0.070	0.037	0.027
703.85	0.054	0.044	0.040	0.024
779.92	0.079	0.064	0.046	0.032
821.26	0.050	0.045	0.040	0.002
827.88	0.059	0.051	0.030	0.015
862.61	0.066	0.054	0.047	0.004
892.37	0.053	0.028	0.025	0.017
922.97	0.073	0.066	0.013	0.005
936.20	0.108	0.066	0.030	0.019

*W and d indicate wavelength and day, respectively.

As is seen in Table 3, the values corresponding to the effective wavelengths for *A. solani* were different for four days. The values for 1 to 4-day had decreasing trends for all effective wavelengths. The values corresponding to the effective wavelengths for 1 to 4 days were in the range of 0.050-0.108, 0.028-0.070, 0.030-0.047, and 0.001-0.032 respectively. The highest values for 1 to 4 days were observed at 936.20, 533.37, 922.97, and 703.85 nm, respectively. The highest differences between the values of 1 and 2-day, 2 and 3-day, and 3 and 4-day were observed at 936.20 (0.108-0.66=0.042), 922.97 (0.066-0.013=0.053), and 862.61 nm (0.047-0.004=0.043), respectively. So, there can be told that the best wavelengths for differentiation of the different days of *A. solani* were 936.2, 922.9, and 862.61 nm.

Table 4. The mean feature value corresponding the effective wavelengths for *A. dumosa* in four days.

W* (nm)	d1	d2	d3	d4
716.21	0.061	0.057	0.046	0.031
853.51	0.061	0.053	0.036	0.004
855.99	0.064	0.029	0.024	0.010
882.45	0.067	0.053	0.017	0.01
888.24	0.078	0.066	0.045	0.044
907.26	0.067	0.063	0.050	0.038
917.18	0.077	0.057	0.037	0.023
920.49	0.069	0.049	0.04	0.021
921.31	0.064	0.036	0.031	0.01
922.14	0.082	0.051	0.045	0.017
927.10	0.075	0.068	0.038	0.012
935.37	0.073	0.053	0.04	0.037
944.46	0.080	0.066	0.048	0.041
947.77	0.088	0.051	0.044	0.034

*W and d indicate wavelength and day, respectively.

Table 4 shows that the values of effective wavelength for *A. dumosa* were different for four days. In all effective wavelengths, the average values for 1 to 4 days had a decreasing trend. The average values of effective wavelength for 1 to 4 days were in the range of 0.061-0.088, 0.029-0.068, 0.017-0.05, and 0.004-0.044, respectively. The highest values for 1 to 4 days were observed at effective wavelengths of 947.77, 922.14, 944.46, 888.24 nm, respectively. Therefore, it can be said that the best wavelength for differentiating different days of *A. dumosa* was 947.77, 922.14, 944.46, 888.24 nm.

Table 5. The mean feature value corresponding the effective wavelengths for *A. atra* in four days.

W* (nm)	d1	d2	d3	d4
780.75	0.051	0.042	0.039	0.032
858.47	0.061	0.032	0.028	0.019
909.79	0.056	0.040	0.024	0.018
913.04	0.055	0.051	0.041	0.018
921.31	0.056	0.04	0.035	0.033
929.58	0.059	0.044	0.043	0.029
932.06	0.086	0.056	0.045	0.038
941.16	0.087	0.051	0.042	0.015
941.98	0.049	0.030	0.025	0.028
943.64	0.065	0.055	0.036	0.025
945.29	0.036	0.034	0.023	0.017

W* and d indicate wavelength and day, respectively.

As can be seen in Table 5, the values of the effective wavelength for *A. atra* were different for four days. In all effective wavelengths, the average values for 1 to 4 days had a decreasing trend. The highest average value was for the effective wavelength of 941.16, which was in the range of 0.015-0.087. And the lowest average value was for the wavelength of 945.29, which was in the range of 0.017-0.036. The highest values for 1 to 4 days were at the effective wavelengths of 941.16, 932.06, 943.64, and 858.47 nm, respectively. Therefore, it can be said that the best wavelength for differentiating different days of *A. atra* was 941.16, 932.06, 943.64, and 858.47 nm.

CONCLUSIONS

In the present study, the effect of day on different fungal isolates and also the comparison of different fungal isolates was done. It is concluded that with increasing the time of enzyme activity, the enzyme activity increased, which causes the color of the solution to become

brighter. That there is a significant difference between different days of enzyme activity. With increasing the duration of enzyme activity, fungal growth increases. Also, in the comparison between different fungal isolates, an observable difference was found between different isolates.

ACKNOWLEDGMENT

The authors thank Plant Protection Department and Mechanical Engineering of Biosystems Department, Ilam University, Ilam, Iran, for supporting the present study.

CONFLICT OF INTEREST STATEMENT

There is no conflict of interest in the present research.

REFERENCES

Abbasi, K., Zafari, D., & Wick, R. (2017). Evaluation of chitinase enzyme in fungal isolates obtained from golden potato cyst nematode (Globodera rostochiensis). *Zemdirbyste-Agriculture*, *104*(2), 179-184. https://doi.org/10.13080/z-a.2017.104.023

Bandumula, N. (2018). Rice production in Asia: Key to global food security. *Proceedings of the National Academy of Sciences, India Section B: Biological Sciences*, *88*(4), 1323-1328. https://doi.org/10.1007/s40011-017-0867-7

Butt, A., Yaseen, S., & Javaid, A. (2011). Seed-borne mycoflora of stored rice grains and its chemical control. *J Anim Plant Sci*, *21*(2), 193-196.

Farokhzad, S., Modaress Motlagh, A., Ahmadi Moghaddam, P., Jalali Honarmand, S., & Kheiralipour, K. (2024). A machine learning system to identify progress level of dry rot disease in potato tuber based on digital thermal image processing. *Scientific Reports*, *14*(1), 1995. https://doi.org/10.1038/s41598-023-50948-x

Gallé, J., & Katzenberger, A. (2025). Indian agriculture under climate change: The competing effect of temperature and rainfall anomalies. *Economics of Disasters and Climate Change*, *9*(1), 53-105. https://doi.org/10.2139/ssrn.4363290

Hosainpour, A., Kheiralipour, K., Nadimi, M., & Paliwal, J. (2022). Quality assessment of dried white mulberry (Morus alba L.) using machine vision. *Horticulturae*, *8*(11), 1011. https://doi.org/10.3390/horticulturae8111011

Khazaee, Y., Kheiralipour, K., Hosainpour, A., Javadikia, H., & Paliwal, J. (2022). Development of a novel image analysis and classification algorithms to separate tubers from clods and stones. *Potato Research*, *65*(3), 707-728. https://doi.org/10.1007/s11540-021-09528-7

Kheiralipour, K., Ahmadi, H., Rajabipour, A., Rafiee, S., & Javan-Nikkhah, M. (2015). Classifying healthy and fungal infected-pistachio kernel by thermal imaging technology. *International Journal of Food Properties*, *18*(1), 93-99. https://doi.org/10.1080/10942912.2012.717155

Kheiralipour, K., Ahmadi, H., Rajabipour, A., Rafiee, S., Javan-Nikkhah, M., & Jayas, D. (2013). Development of a new threshold based classification model for analyzing thermal imaging data to detect fungal infection of pistachio kernel. *Agricultural Research*, *2*(2), 127-131. https://doi.org/10.1007/s40003-013-0057-7

Kheiralipour, K., Ahmadi, H., Rajabipour, A., Rafiee, S., Javan-Nikkhah, M., Jayas, D. S., Siliveu, K., & Malihipour, A. (2021). Processing the hyperspectral images for detecting infection of pistachio kernel by R5 and KK11 isolates of Aspergillus flavus fungus. *Iran. J. Biosyst. Eng*, *52*(1), 13-25.

Kheiralipour, K., & Jayas, D. S. (2023). Advances in image processing applications for assessing leafy materials. *International Journal of Tropical Agriculture*, *41*, 31-47.

Kheiralipour, K., & Nargesi, M. H. (2024). Classification of wheat flour levels in powdered spices using visual imaging. *Journal of Agriculture and Food Research*, *18*, 101408. https://doi.org/10.1016/j.jafr.2024.101408

Kumar, A., Bharti, V., Kumar, V., Kumar, U., & Meena, P. (2016). Hyperspectral imaging: A potential tool for monitoring crop infestation, crop yield and macronutrient analysis, with special emphasis to Oilseed Brassica. *Journal of Oilseed Brassica*, *7*(2), 113-125.

Kunjaroenruk, J., Koonmanee, S., Singkham, N., Chankaew, S., & Suriharn, K. (2025). Genotypic variation and seasonal effects on rice (Oryza sativa L.) grain protein content and yield in tropical Savannah environment. *Journal of Agriculture and Food Research*, *20*, 101778. https://doi.org/10.1016/j.jafr.2025.101778

Kusai, N. A., Azmi, M. M. Z., Zainudin, N. A. I. M., Yusof, M. T., & Razak, A. A. (2016). Morphological and molecular characterization, sexual reproduction, and pathogenicity of Setosphaeria rostrata isolates from rice leaf spot. *Mycologia*, *108*(5), 905-914. https://doi.org/10.3852/15-175

Liu, C., Lu, W., Gao, B., Kimura, H., Li, Y., & Wang, J. (2020). Rapid identification of chrysanthemum teas by computer vision and deep learning. *Food Science & Nutrition*, *8*(4), 1968-1977. https://doi.org/10.1002/fsn3.1484

Monreal, J., & Reese, E. T. (1969). The chitinase of Serratia marcescens. *Canadian journal of microbiology*, *15*(7), 689-696. https://doi.org/10.1139/m69-122

Nahar, A., Luckstead, J., Wailes, E. J., & Alam, M. J. (2018). An assessment of the potential impact of climate change on rice farmers and markets in Bangladesh. *Climatic Change*, *150*(3), 289-304. https://doi.org/10.1007/s10584-018-2267-2

Nargesi, M. H., Amiriparian, J., Bagherpour, H., & Kheiralipour, K. (2024). Detection of different adulteration in cinnamon powder using hyperspectral imaging and artificial neural network method. *Results in Chemistry*, *9*, 101644. https://doi.org/10.1016/j.rechem.2024.101644

Nargesi, M. H., Heidarbeigi, K., Moradi, Z., & Abdolahi, S. (2025). Detection of chlorine in potassium chloride and potassium sulfate using chemical imaging and artificial neural network. *Spectrochimica Acta Part A: Molecular and Biomolecular Spectroscopy*, *326*, 125253. https://doi.org/10.1016/j.saa.2024.125253

Nargesi, M. H., & Kheiralipour, K. (2024a). Ability of visible imaging and machine learning in detection of chickpea flour adulterant in original cinnamon and pepper powders. *Heliyon*, *10*(16). https://doi.org/10.1016/j.heliyon.2024.e35944

Nargesi, M. H., & Kheiralipour, K. (2024b). Visible feature engineering to detect fraud in black and red peppers. *Scientific Reports*, *14*(1), 25417. https://doi.org/10.1038/s41598-024-76617-1

Terensan, S., Fernando, H. N. S., Silva, J. N., Perera, S. C. N., Kottearachchi, N. S., & Weerasena, O. J. (2021). In silico molecular and morphological analysis of rice blast resistant gene Pi-ta in Sri Lankan rice germplasm. *Journal of Genetic Engineering and Biotechnology*, *19*(1), 163. https://doi.org/10.1186/s43141-021-00239-7

Tikhonov, V. E., Lopez-Llorca, L. V., Salinas, J., & Jansson, H.-B. (2002). Purification and characterization of chitinases from the nematophagous fungi Verticillium chlamydosporium and V. suchlasporium. *Fungal Genetics and Biology*, *35*(1), 67-78. https://doi.org/10.1006/fgbi.2001.1312

Vejarano, R., Siche, R., & Tesfaye, W. (2017). Evaluation of biological contaminants in foods by hyperspectral imaging: A review. *International journal of food properties*, *20*(2), 1264-1297. https://doi.org/10.1080/10942912.2017.1338729